# Structural, electrical, and optical properties of $InAs_xSb_{1-x}$ epitaxial films grown by liquid-phase epitaxy

Fubao Gao,[1,a)] NuoFu Chen,[1,2] X. W. Zhang,[1] Yu Wang,[1] Lei Liu,[1] Zhigang Yin,[1] and Jinliang Wu[1]

[1]*Key Laboratory of Semiconductor Materials Science, Institute of Semiconductors, Chinese Academy of Sciences, P.O. Box 912, Beijing 100083, People's Republic of China*

[2]*National Laboratory of Microgravity, Institute of Mechanics, Chinese Academy of Sciences, Beijing 100080, People's Republic of China*

(Received 28 February 2008; accepted 12 August 2008; published online 2 October 2008)

The $InAs_xSb_{1-x}$ films were grown on (100) GaSb substrates by liquid-phase epitaxy, and their structural, electrical, and optical properties were investigated. The high-resolution x-ray diffraction results reveal that the single crystalline $InAs_xSb_{1-x}$ films with a midrange composition are epitaxially grown on the GaSb substrates. Temperature dependence of the Hall mobility was theoretically modeled by considering several predominant scattering mechanisms. The results indicate that ionized impurity and dislocation scatterings dominate at low temperatures, while polar optical phonon scattering is important at room temperature (RT). Furthermore, the $InAs_xSb_{1-x}$ films with the higher As composition exhibit the better crystalline quality and the higher mobility. The $InAs_{0.35}Sb_{0.65}$ film exhibits a Hall mobility of $4.62\times10^4$ $cm^2\ V^{-1}\ s^{-1}$. The cutoff wavelength of photoresponse is extended to about 12 $\mu$m with a maximum responsivity of 0.21 V/W at RT, showing great potential for RT long-wavelength infrared detection. © *2008 American Institute of Physics*. [DOI: 10.1063/1.2989116]

## I. INTRODUCTION

Long-wavelength (8–12 $\mu$m) infrared detectors that can operate at room temperature (RT) have attracted much interest in the past years due to their important applications. At present, $Hg_{1-x}Cd_xTe$ is the most prevalent material in high-performance, long-wavelength infrared detectors. However, it suffers from instability and nonuniformity over a large area due to the weakness of mercury bonding in the compound[1] and high mercury vapor pressure during material growth,[2] respectively. $InAs_xSb_{1-x}$ is more stable, and has higher electron and hole mobilities than $Hg_{1-x}Cd_xTe$, and more importantly, when the value of $x$ is in the midrange ($0.2<x<0.7$) it exhibits a large, positive "optical bowing" effect with a minimum band gap of 0.1 eV near $x=0.35$. Thus, the $InAs_xSb_{1-x}$ alloy is a promising material for the realization of low-cost RT detectors operating in the 3–5 and 8–12 $\mu$m windows where the atmospheric absorption is minimal.[3–6]

For the $InAs_xSb_{1-x}$ film growth, some III-V compound semiconductors, such as GaAs, GaSb, InAs, and InSb, can be used for substrates. Among these semiconductors, GaSb is considered to be the most promising substrate material for growing $InAs_xSb_{1-x}$ film because of its less lattice mismatch with $InAs_xSb_{1-x}$ and appropriate melting point. As is much more accessible and economical than molecular beam epitaxy (MBE) (Refs. 7–10) and metal organic chemical vapor deposition (MOCVD),[11–13] liquid-phase epitaxy (LPE) is often considered for the growth of $InAs_xSb_{1-x}$ films. Recently, Bansal and co-workers[14,15] have reported successful epitaxial growth of $InAs_xSb_{1-x}$/GaAs by LPE with extremely low ramp-cooling rates, but only 6 at. % arsenic was incorporated into the $InAs_xSb_{1-x}$ films due to the miscibility gap. This obstructs their $InAs_xSb_{1-x}$/GaAs from being applied above the 9.5 $\mu$m wavelength range. More recently, we have demonstrated that high quality epitaxial growth of $InAs_xSb_{1-x}$ films with a midrange composition ($x=0.3$) on GaSb can be obtained using an $InAs_{0.91}Sb_{0.09}$ buffer layer lattice matched to GaSb substrates by LPE technique.[16] Using these epitaxial films, a comprehensive investigation of electrical and optical properties of $InAs_xSb_{1-x}$ epitaxial layers with a midrange composition becomes possible and is the purpose of the present study.

## II. EXPERIMENTAL PROCEDURE

$InAs_xSb_{1-x}$ films were grown by a conventional horizontal graphite sliding-boat system with an ambient of flowing Pd membrane-purified hydrogen at atmospheric pressure in a quartz reactor tube, which has already been described in detail elsewhere.[17] The starting materials were 6*N* pure In, Sb, and undoped polycrystalline InAs. The substrates were well-polished *n*-type (100) GaSb wafers with the size of $10\times8\times0.5$ $mm^3$. The $InAs_xSb_{1-x}$ films were grown by a step cooling method, and the optimum conditions were adopted according to our previous work.[16] To allow the source materials to get proper homogenization, they were heated to 700 °C for 3 h together. After the temperature was cooled down to the loading temperature of 590 °C, the GaSb substrates were put into the boat. Subsequently, the temperature was cooled further down to the growth temperature ($T_G$), and the source melt was pushed onto the surface of the substrate. Constant growth temperature helps the uniformity of the $InAs_xSb_{1-x}$ films in the growth direction. The growth

[a)]aElectronic mail: fbgao@semi.ac.cn.

 

TABLE I. The growth parameters and characterization results for the three $InAs_xSb_{1-x}$ films. Band gaps ($E_g$) obtained from the FTIR data for the $InAs_xSb_{1-x}$ films. $E_{g,w}$ denotes band gaps at 300 K calculated from the equation of Woolley and Warner (Ref. 29).

| Sample ID | III-V ratio (In:InAs:Sb) | $T_G$ (°C) | Composition ($x$) | XRD FWHM (arc) | $\mu$ (300K) ($cm^2\ V^{-1}\ s^{-1}$) | $n$ (300K) ($cm^{-3}$) | $E_g$ (eV) | $E_{g,w}$ (eV) |
|---|---|---|---|---|---|---|---|---|
| A | 1:0.29:0.087 | 429 | 0.08 | 0.88 | $4.60\times10^4$ | $2.5\times10^{16}$ | 0.130 | 0.145 |
| B | 1:1.06:0.036 | 549 | 0.30 | 0.59 | $4.20\times10^4$ | $2.8\times10^{16}$ | 0.116 | 0.102 |
| C | 1:1.06:0.040 | 551 | 0.35 | 0.50 | $4.62\times10^4$ | $4.2\times10^{16}$ | 0.108 | 0.100 |

time of the $InAs_xSb_{1-x}$ epilayers ranged from 10 to 20 min. Finally, the substrate was slid out of the melt, and then the quartz reactor tube with the graphite boat was drawn out of the furnace. Three samples were prepared under the different conditions, and the basic growth parameters are summarized in Table I.

For the x-ray diffraction (XRD) measurements in a $\theta$-$2\theta$ mode, a Panalytical X'Pert-MPD Pro diffractometer with a Cu $K\alpha$ x-ray source was used. Besides the conventional $\theta$-$2\theta$ mode, the rocking curving ($\omega$ scans) and azimuthal scans ($\Phi$ scans) were also taken by a high-resolution Bede-D1 diffractometer to determine crystalline quality of $InAs_xSb_{1-x}$ films further. The alloy concentration was determined by energy dispersive x-ray analysis (EDAX) and also from Vegard's law based on XRD results. Electrical properties were examined by Hall measurements. Fourier transform infrared (FTIR) spectra were taken at RT by a Bruker spectrometer (Tensor 27) with a resolution of 4 $cm^{-1}$. For Hall measurements, as well as FTIR and rocking curve characterizations, the substrates with the buffer layers were removed by grinding with emery grinding powder in order to eliminate their effects. To control the amount of grinding, a precision thickness gauge with an accuracy of $\pm1$ $\mu$m was used to check the remained epilayer thickness, and the complete removal of the substrates was confirmed by the results of XRD.

## III. RESULTS AND DISCUSSION

Three $InAs_xSb_{1-x}$ films under different conditions were grown on $n$-type (100) GaSb substrates with a buffer layer of $InAs_{0.91}Sb_{0.09}$ by LPE. Because of the high melting point and the good stability of the $InAs_{0.91}Sb_{0.09}$ layer,[18] the substrate dissolution and element interdiffusion in the interface could be avoided, which has been verified by scanning electronic microscopy and the linescan of EDAX.[16] To determine the structural properties, the $InAs_xSb_{1-x}$ films were examined by XRD in a normal $\theta$-$2\theta$ configuration, and the corresponding XRD patterns are presented in Fig. 1 together with an enlarged view given as inset to emphasize the shifts of the XRD peaks. To demonstrate the epitaxial relationship between the $InAs_xSb_{1-x}$ film and the GaSb substrate, the GaSb substrate of sample B was not removed completely for the XRD measurement. Besides the diffraction peaks from the (100) GaSb substrate at 29.27° and 60.72°, only two peaks occurred at ~28° and ~58°, corresponding to the (200) and (400) diffraction of the zinc-blende structural $InAs_xSb_{1-x}$, respectively, which clearly indicates that the (100) planes of the $InAs_xSb_{1-x}$ films are oriented parallel to the (100) GaSb surface. Furthermore, from the inset one can see that the position of the (400) reflection peaks varies from sample to sample, indicating different As compositions for the three samples.

In general, Vegard's law is used to calculate the compositions of $InAs_xSb_{1-x}$ alloys; however, some uncertainties in the validity of Vegard's law have been reported.[19] In order to verify the accuracy of Vegard's law, we used a model suggested by Chen *et al.*[20] to analyze the correlation between the As composition and lattice parameters. In an ideal $InAs_xSb_{1-x}$ alloy, it is reasonable to assume that every incorporated As atom occupies a substitutional Sb site. The lattice strain $\Delta a/a$ due to the As atom incorporation is given by[20]

$$\frac{\Delta a}{a} = \frac{C_{11}+2C_{12}}{C_{11}} \frac{r_{As}-r_{Sb}}{r_{In}+r_{Sb}} \frac{x}{2}, \tag{1}$$

where $r_{In}$, $r_{As}$, and $r_{Sb}$ are the Pauling covalent radii of In, As, and Sb, respectively, and $C_{11}=6.67\times10^{11}$ dyn/cm$^2$ and $C_{12}=3.65\times10^{11}$ dyn/cm$^2$. The As compositions calculated from this model, as shown in Table I, are consistent with those obtained from EDAX. The results are also similar to the predictions of Vegard's law, and the maximum error between the calculated compositions from the model and Vegard's law is ~3%.

To further confirm epitaxial growth and extract the in-plane orientation of the prepared $InAs_xSb_{1-x}$ film, XRD azimuthal scans from 0° to 360° were taken on the out-of-plane $InAs_xSb_{1-x}$ (115) reflections at 17° to the sample surface (100). An example for sample C ($InAs_{0.35}Sb_{0.65}$ film) is presented in Fig. 2(a). As seen in Fig. 2(a) the $\varphi$ scan over 360° azimuths gives four sharp peaks separated by 90° intervals

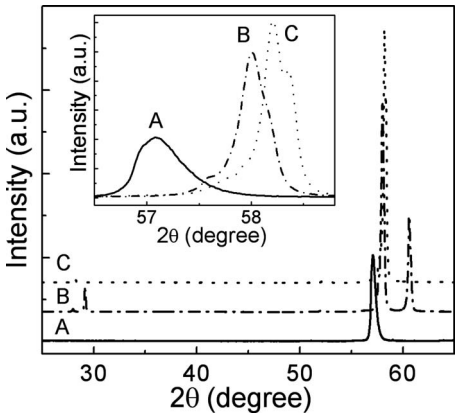


FIG. 1. XRD patterns of the $InAs_xSb_{1-x}$ samples in the $\theta$-$2\theta$ mode. The inset shows an enlarged view for (400) peaks of the samples.

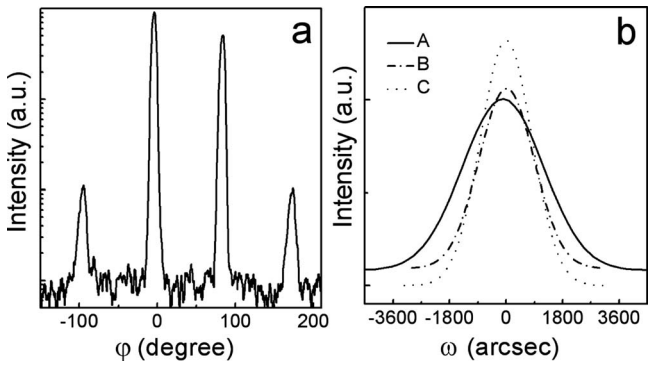


FIG. 2. HRXRD patterns of the $InAs_xSb_{1-x}$ samples. (a) Azimuthal scans of the $InAs_{0.35}Sb_{0.65}$ (115) reflection for sample C. (b) Rocking curves of the three $InAs_xSb_{1-x}$ films.

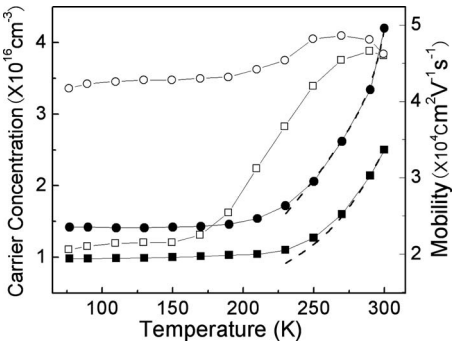


FIG. 3. Temperature dependence of the carrier concentration (solid symbols) and the Hall mobility (open symbols) for sample A ($InAs_{0.08}Sb_{0.92}$, squares) and sample C ($InAs_{0.35}Sb_{0.65}$, circles). The dashed lines are the fitting results of $n_H$.

with negligible scattering in between them, reflecting a fourfold symmetry, as would be expected for a [100] axis of a perfect InAsSb single crystal.

To judge the epitaxial quality of the $InAs_xSb_{1-x}$ films, the rocking curves of the $InAs_xSb_{1-x}$ (400) reflection were recorded using a high-resolution diffractometer. Figure 2(b) shows the rocking curves of the three $InAs_xSb_{1-x}$ films. The full widths at half maximum (FWHMs) of the (400) rocking curves are 0.88°, 0.59°, and 0.5° for samples A, B, and C, respectively. The FWHM values are higher for the all three samples due to the larger lattice mismatch between the $InAs_xSb_{1-x}$ films and the $InAs_{0.91}Sb_{0.09}$ buffer layer. In our case, the values of lattice mismatch between the $InAs_xSb_{1-x}$ films and the $InAs_{0.91}Sb_{0.09}$ buffer layer vary from 3.8% to 5.6% in the composition range $x=0.08-0.35$, and so large lattice mismatch creates misfit strains or dislocations,[21,22] and the crystallinity of the films is degraded. On the other hand, it can be seen that the FWHMs of the rocking curves decrease with increasing As composition in the $InAs_xSb_{1-x}$ films, indicating an improved crystal quality with $x$, which can be due to the less lattice mismatch between $InAs_xSb_{1-x}$ and the $InAs_{0.91}Sb_{0.09}$ buffer layer when more As atoms were incorporated into the alloy.

Hall measurements were performed on the samples without GaSb substrates by the van der Paw method, and Ohmic contacts were made with indium solder. All the samples are $n$-type conductive. The carrier concentrations (solid symbols) as functions of temperature for samples A and C are plotted in Fig. 3, respectively. It can be seen from Fig. 3 that at low temperatures ($\leq$210 K), the carrier concentrations were kept almost constant, implying that impurities of shallow donors are ionized completely within this temperature range. The samples become intrinsic after around 210 K, and an exponential increase in carrier concentration $n$ is observed. For an intrinsic semiconductor, the free electron concentration of $n$-type semiconductors can be approximately considered as the following:[23] $n=N_D/2+n_i$, where $N_D$ is the shallow donor concentration and $n_i$ is the intrinsic carrier concentration with a temperature dependence $n_i \propto T^{3/2} \exp[-E_g/(2kT)]$. Because the hole mobility is much lower than the electron mobility, the contribution from the hole can be safely ignored. Therefore, the Hall carrier concentration $n_H$ can be approximately expressed as

$$n_H \approx n = N_D/2 + A \times T^{3/2} \times \exp(-E_g/(2kT)), \quad (2)$$

where $A$ is a constant and $E_g$ is the band gap. The temperature dependence of $E_g$ can be expressed by Varshni's equation,[14]

$$E_g = E_g(0) + \alpha T^2/(\beta + T), \quad (3)$$

where $\alpha=3.01\times10^{-4}$ eV K$^{-1}$ and $\beta=341$ K. $E_g(0)$ is the energy band gap at 0 K, and $E_g(0)$ are 0.198 and 0.138 eV for $x=0.08$ and 0.35, respectively. According to Eqs. (2) and (3), the temperature dependence of $n_H$ was fitted at higher temperatures ($\geq$210 K), and the corresponding results of $n_{\text{fit}}$ are given in Fig. 3 as dashed lines. The fitted curves are in good agreement with experimental data. The values of $N_D$ extracted from the fitted results are $1.6\times10^{16}$ and $9.0\times10^{15}$ cm$^{-3}$ for samples A and C, respectively, which are close to the measured carrier concentrations $n_H$ at low temperatures. These results support the proposal that at low temperatures, impurities of shallow donor are ionized completely and $n_H \approx N_D$.

The temperature dependence of the Hall mobility (open symbols) for sample A ($InAs_{0.08}Sb_{0.92}$) and sample C ($InAs_{0.35}Sb_{0.65}$) is also illustrated in Fig. 3. The mobilities initially increase and then gradually decrease with temperature, and the maximum values of $4.66\times10^4$ and $4.86\times10^4$ cm$^2$ V$^{-1}$ s$^{-1}$ appear at around 290 and 270 K for samples A and C, respectively. The mobility of the $InAs_{0.35}Sb_{0.65}$ film grown on GaSb was as high as $4.62\times10^4$ cm$^2$ V$^{-1}$ s$^{-1}$ with a carrier concentration ($n$ type) of $4.2\times10^{16}$ cm$^{-3}$ at RT. These results are even better than those reported for epitaxial $InAs_xSb_{1-x}$ films with similar composition grown by MOCVD (Ref. 2) and MBE.[8,24] The electron mobility at RT is strongly affected by scattering of the crystal lattice. Thus a high electron mobility at RT proved that the lattice perfection of the $InAs_{0.35}Sb_{0.65}$ epitaxial layer is quite good. Furthermore, the mobility of the $InAs_{0.08}Sb_{0.92}$ film is much smaller than that of the $InAs_{0.35}Sb_{0.65}$ film at low temperatures.

The electron mobility can be calculated by the momentum relaxation time approximation (RTA) method and Matthiessen's rule. In RTA, the individual mobility due to a scattering process, $i$, is given by

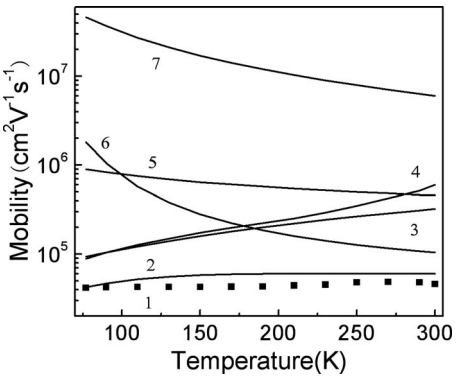


FIG. 4. Contributions to mobility from different scattering mechanisms for sample C ($InAs_{0.35}Sb_{0.65}$): (1) experimental data, (2) total calculated, (3) ionized impurity, (4) dislocations, (5) alloy disorder, (6) polar optical phonons, and (7) acoustic phonons.

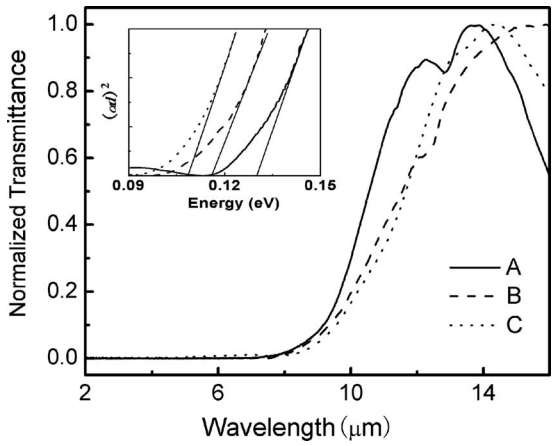


FIG. 5. FTIR spectra at RT of the three $InAs_xSb_{1-x}$ films. The inset shows the corresponding $(\alpha d)^2$ for linear fittings.

$$\mu_i = \frac{q\langle \tau_m \rangle^i}{m^*}, \tag{4}$$

where $m^*$ is the effective mass and $\langle \tau_m \rangle$ is the momentum relaxation time. Then the overall combined mobility $\mu_t$ can be calculated according to Matthiessen's rule,

$$\mu_t = \left[ \Sigma_i \frac{1}{\mu_i} \right]^{-1}. \tag{5}$$

The scattering mechanisms that may be significant in the ternary compound semiconductors include the following: ionized impurity, alloy, dislocation, acoustic phonon, polar optical phonon, piezoelectric, and carrier-carrier scatterings. Their relative contributions depend on temperature, carrier concentration, and alloy composition.[15,25] We have calculated the electron mobility for sample C ($InAs_{0.35}Sb_{65}$ film) according to Matthiessen's rule by considering predominant scattering mechanisms. A theoretical fit along with the experimental data for sample C is shown in Fig. 4, where relative contributions from ionized impurity, polar optical phonon, dislocation, alloy, and acoustic phonon scatterings are shown. It is found that at low temperatures ionized impurity and dislocation scattering become the predominant mobility-limiting mechanisms. Moreover at higher temperatures polar optical phonon scattering becomes important in determining its temperature dependence. The effects of alloy and acoustic phonon scattering have been found to be negligible in the entire temperature range of the simulation.

According to Fig. 4, the ionized impurity and dislocation scatterings are the most significant scattering mechanism at low temperatures. However, the mobility of sample C with higher $N_D$ is higher than that of sample A. The absence of a correlation of mobility with background doping implies that the effect of dislocation is more apparent for the low-temperature mobility. The large dislocation density (as found from high resolution XRD (HRXRD) in these films) may also be taken as an indirect evidence for a strong role of dislocation scattering at low temperatures.[15] Furthermore, the low-temperature mobility of sample C ($InAs_{0.35}Sb_{0.65}$ film) is higher than that of sample A ($InAs_{0.08}Sb_{0.92}$ film), as shown in Fig. 4, which can be understood by using the dislocation scattering mechanism. Because of the larger lattice mismatch between the $InAs_{0.08}Sb_{0.92}$ film and the $InAs_{0.91}Sb_{0.09}$ buffer layer, the dislocation density in sample A is higher, as indicated by the broader rocking curve, and thus the electron mobility is also degraded significantly.

The mobility at RT is mainly limited by polar optical phonon scattering, which predicts a RT mobility of around $6.0\times10^4$ $cm^2\ V^{-1}\ s^{-1}$, which is higher than the measured RT mobility of $4.62\times10^4$ $cm^2\ V^{-1}\ s^{-1}$. The discrepancy in experimental data and theoretically calculated values is observed within the temperature range of $\geq 100$ K, indicating that the scattering process of the alloy is far more complex than that considered by the usual scattering theories. The other scattering mechanisms, such as piezoelectric, carrier-carrier, and double-phonon scatterings, that are not taken into account in the above calculation may contribute to the total mobility. Additionally, the interaction of the various scattering mechanisms has been ignored, and the material parameters used in the calculation may deviate from that of the actual crystal. All of them may be responsible for this discrepancy.[26–28]

The normalized FTIR transmission spectra of the three samples are shown in Fig. 5. The absorption edges of the $InAs_xSb_{1-x}$ films shift toward the long-wavelength side with the increase of $x$, indicating the dependence of band gap with composition. For a direct energy gap semiconductor, the absorption coefficient $\alpha$ of $InAs_xSb_{1-x}$ can be described as $\alpha=A(h\nu-E_g)^{1/2}$, which corresponds to the experimental data on the absorption edge. Here $\alpha$ is the absorption coefficient in $cm^{-1}$, $\nu$ is the incident photon frequency, and $A$ is a constant depending on the electron and hole effective masses and the optical transition matrix element. Therefore, based on the data of $\alpha d$ ($d$ is the film thickness) calculated from the FTIR transmission results, $E_g$ at RT can be obtained from the linear fitting of $(\alpha d)^2$ (as shown in the inset of Fig. 5) and is presented in Table I. The band gap $E_g$ for sample A ($InAs_{0.08}Sb_{0.92}$ film) is 0.13 eV at RT, and it reduces to 0.108 eV for sample C, demonstrating a strong positive optical bowing effect. On the other hand, the dependence of the band gap on the composition of $InAs_xSb_{1-x}$ at RT has been given by Woolley and Warner[29] as $E_{g,w}(x)$

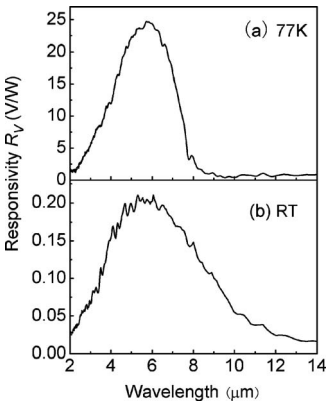


FIG. 6. Spectral responsivity of the photoconductors fabricated on sample C at (a) 77 K and (b) RT.

$=0.35-0.771(1-x)+0.596(1-x)^2$(eV). The band gap calculated from this equation ($E_{g,w}$), also listed in Table I, deviates from $E_g$ obtained from the FTIR data. The band gap of $InAs_xSb_{1-x}$ may be influenced by the degree of ordering,[3] the band tailing,[30] or residual strain[31] in the alloy, so the discrepancy may be attributed to the difference between growth processes in producing ordering and residual strain. Additionally, Bansal *et al.*[32] found that the absorption spectrum of $InAs_{0.05}Sb_{0.95}$ can be separated into three distinct regions corresponding to the free carrier absorption, the Urbach edge absorption, and the direct interband absorption across the energy gap. In this work, the free carrier absorption at smaller energies (longer wavelength) can also be observed in Fig. 5.

Photoconductors formed by $0.1\times2$ mm$^2$ bars of $InAs_xSb_{1-x}$ films were fabricated on sample C. The spectral photoresponse was measured at 77 K and RT using a FTIR spectrometer, and the absolute responsivity was calibrated based on the responsivity measurement at 77 K using a standard blackbody source with a temperature of 800 K. The bias voltage applied to the photoconductors was 1.5 V. Figures 6(a) and 6(b) show the spectral responsivities of the photoconductors at 77 K and RT, respectively. A notable photoresponse beyond 8 $\mu$m is observed with both photoconductors at RT, and the cutoff wavelength is extended to about 12 $\mu$m with a maximum responsivity of 0.21 V/W at RT, showing great potential for RT long-wavelength infrared detection. This indicates that the photoresponse of sample C can cover the long-wavelength transmission window in the atmosphere, making its application in long-wavelength infrared detection possible.

## IV. CONCLUSION

The structural, electrical, and optical absorptions in $InAs_xSb_{1-x}$ films grown by LPE on (100) GaSb substrates with an $InAs_{0.91}Sb_{0.09}$ buffer layer were investigated with XRD, Hall, and FTIR measurements. The results show that the $InAs_xSb_{1-x}$ films with the higher As composition exhibit the better crystalline quality, the wider band gap, and the higher mobility. The $InAs_{0.35}Sb_{0.65}$ film exhibits a Hall mobility of $4.62\times10^4$ cm$^2$ V$^{-1}$ s$^{-1}$ and a cutoff wavelength of 12 $\mu$m at RT, indicating the high quality of the films and potential infrared applications in the long wavelength. The temperature dependence of the Hall mobility was modeled theoretically, and the results indicate that ionized impurity and dislocation scatterings are significant at low temperatures, while polar optical phonon scattering is important at RT. The effects of acoustic phonon scattering have been found to be negligible below 300 K.

## ACKNOWLEDGMENTS

This work was supported by Special Funds for Major State Basic Research Project No. 2002CB311905 and by the National Natural Science Foundation of China (Grant No. 60576010).

[1] T. Niedziela and R. Ciupa, Solid-State Electron. **45**, 41 (2001).
[2] J. D. Kim, D. Wu, J. Wojkowski, J. Piotrowski, J. Xu, and M. Razeghi, Appl. Phys. Lett. **68**, 99 (1996).
[3] S.-H. Wei and A. Zunger, Appl. Phys. Lett. **58**, 2684 (1991).
[4] G. P. Srivastava, J. L. Martins, and A. Zunger, Phys. Rev. B **31**, 2561 (1985).
[5] H. R. Jen, K. Y. Ma, and G. B. Stringfellow, Appl. Phys. Lett. **54**, 1154 (1989).
[6] S. R. Kurtz, L. R. Dawson, R. M. Biefeld, D. M. Follstaedt, and B. L. Doyle, Phys. Rev. B **46**, 1909 (1992).
[7] M. Y. Yen, B. F. Levine, C. G. Bethea, K. K. Choi, and A. Y. Cho, Appl. Phys. Lett. **50**, 927 (1987).
[8] M. Y. Yen, R. People, and K. W. Wecht, J. Appl. Phys. **64**, 952 (1988).
[9] J.-I. Chyi, S. Kalem, N. S. Kumar, C. W. Litton, and H. Morkoc, Appl. Phys. Lett. **53**, 1092 (1988).
[10] S. Tsukamoto, P. Bhattacharya, Y. C. Chen, and J. H. Kim, J. Appl. Phys. **67**, 6819 (1990).
[11] P. K. Chiang and S. M. Bedair, J. Electrochem. Soc. **131**, 2422 (1984).
[12] P. K. Chiang and S. M. Bedair, Appl. Phys. Lett. **46**, 383 (1985).
[13] R. M. Biefeld, C. R. Hills, and S. R. Lee, J. Cryst. Growth **91**, 515 (1988).
[14] V. K. Dixit, B. Bansal, V. Venkataraman, H. L. Bhat, K. S. Chandrasekharan, and B. M. Arora, J. Appl. Phys. **96**, 4989 (2004).
[15] B. Bansal, V. K. Dixit, V. Venkataraman, and H. L. Bhat, Physica E (Amsterdam) **20**, 272 (2004).
[16] F. B. Gao, N. F. Chen, L. Liu, X. W. Zhang, J. L. Wu, and Z. G. Yin, J. Cryst. Growth **304**, 472 (2007).
[17] C. T. Peng, N. F. Chen, F. B. Gao, X. W. Zhang, C. L. Chen, J. L. Wu, and Y. D. Yu, Appl. Phys. Lett. **88**, 242108 (2006).
[18] Y. Mao and A. Krier, J. Cryst. Growth **133**, 108 (1993).
[19] S. Z. Wang, S. F. Yoon, W. J. Fan, W. K. Loke, and T. K. Ng, J. Appl. Phys. **96**, 2010 (2004).
[20] N. F. Chen, Y. T. Wang, H. J. He, and L. Y. Lin, Phys. Rev. B **54**, 8516 (1996).
[21] H. C. Gao, W. X. Wang, Z. W. Jiang, L. S. Liu, J. M. Zhou, and H. Chen, J. Cryst. Growth **308**, 406 (2007).
[22] K. Yuan, K. Radhakrishnan, H. Q. Zheng, Q. D. Zhuang, and G. I. Ing, Thin Solid Films **391**, 36 (2001).
[23] N. K. Liu, B. S. Zhu, and J. S. Luo, *Semiconductor Physics*, 2nd ed. (Electronics Industry, Beijing, 2003), p. 84.
[24] C. G. Bethea, M. Y. Yen, B. F. Levine, and K. K. Choi, Appl. Phys. Lett. **51**, 1431 (1987).
[25] R. J. Egan, V. W. L. Chin, and T. L. Tansley, J. Appl. Phys. **75**, 2473 (1994).
[26] V. W. L. Chin, R. J. Egan, and T. L. Tansley, J. Appl. Phys. **69**, 3571 (1991).
[27] C. Besikci, Y. H. Choi, G. Labeyrie, E. Bigan, and M. Razaghi, J. Appl. Phys. **76**, 5820 (1994).
[28] V. W. L. Chin, R. J. Egan, and T. L. Tansley, J. Appl. Phys. **72**, 1410 (1992).
[29] J. C. Woolley and J. Warner, Can. J. Phys. **42**, 1879 (1964).
[30] R. Chtourou, F. Bousbih, S. B. Bouzid, F. F. Charfi, J. C. Harmand, G. Ungaro, and L. Largeau, Appl. Phys. Lett. **80**, 2075 (2002).
[31] See, e.g., S. Adachi, *Physical Properties of III-V Semiconductor Compounds* (Wiley, New York, 1992), p. 275.
[32] B. Bansal, V. K. Dixit, V. Venkataraman, and H. L. Bhat, Appl. Phys. Lett. **90**, 101905 (2007).